Particle Size Sorting of TiO_2 Powders Synthesized via Ultrasonic Atomization–Pyrolysis and Its Influence on Gas Sensing Properties

Shanabhau D. Bagul *

Nanomaterials Research Laboratory, Department of Physics, Pratap College, Amalner, Maharashtra, India

Editor's note: Air quality is vital for the health of humans and ecosystems. Pollutants like NO_2, produced by fossil fuel combustion, pose serious health risks and environmental challenges. This is the reason for the great global interest in effective sensors for detecting NO_2. Bagul synthesized titanium dioxide (TiO_2) powders using ultrasonic atomization and pyrolysis. The resulting powders were characterized using X-ray diffraction and scanning electron microscopy. Sensor testing showed that the optimum TiO_2-based sensor exhibited high sensitivity to NO_2 gas at an optimal temperature of 250°C, with a quick response time of 2 seconds and recovery in 23 seconds.

doi: 10.22034/jams.2026.260304

How to cite: S.D. Bagul, *Journal of Applied Material Science*, **2026**, *2*, 260304.

JOURNAL OF
APPLIED
MATERIAL
SCIENCE
jams.hsu.ac.ir

Journal of Applied Material Science **2026**, 2, 260304
How to cite: S.D. Bagul, *Journal of Applied Material Science*, **2026**, 2, 260304.
Journal homepage: **jams.hsu.ac.ir**

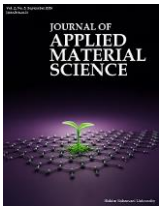

Original Research

Particle Size Sorting of TiO_2 Powders Synthesized via Ultrasonic Atomization–Pyrolysis and Its Influence on Gas Sensing Properties

Shanabhau D. Bagul *

Nanomaterials Research Laboratory, Department of Physics, Pratap College, Amalner, Maharashtra, India

Abstract

In this work, titanium dioxide (TiO_2) powder is synthesized using the ultrasonic atomization and pyrolysis technique. An ultrasonic atomizer having a resonance frequency of 2.4 MHz is used to convert the solution into fine mist. The mist was pushed into the horizontal double-zone quartz reactor furnace, and the pyrolysis temperature was optimized to get nanocrystalline powder. The prepared powders were collected into the traps attached to the rear end of the furnace. The powder named TiO_2_T1, TiO_2_T2, and TiO_2_T3, respectively, for the powders collected in traps 1, 2, and 3. The powders were analyzed by various characterization techniques such as X-ray diffraction to get their structural characteristics and scanning electron microscopy for microstructural information. The optical properties were analyzed by UV-Visible and photoluminescence spectroscopy. Thermal properties of the powders were studied by a simultaneous thermal analyzer. Thick films of the powders were prepared by the screen-printing method, and sensors were fabricated and tested for various gases. The sensor prepared from the powder collected in trap T3, i.e., TiO_2_T3, shows the highest response to NO_2 gas compared to the other sensors. The sensor also shows good response-recovery time. The results are analyzed and concluded in this article.

Keywords: TiO_2 powder; Hollow microsphere; Ultrasonic atomization; Gas sensor; Pyrolysis.

1. Introduction

Air quality is an important concern for the health of not only human being also living organisms such as plants and animals. Air quality control and monitoring are necessary to prevent the atmosphere from pollution. In the last 2-3 decades, the world has produced a large amount of pollution due to the development of chemical and aviation industries. There is an urgent need to develop good-quality sensors to measure pollutant gases. The major components of air pollution are NO_2, SO_2, CO_2, etc. NO_2 is produced from incomplete combustion of fossil fuels and vehicle exhaust and causes most respiratory problems in human beings, also effects on ozone layer of the atmosphere, and produces greenhouse effects, which increase temperature [1]. People have realized the effect of NO_2 on the environment due to industrial waste and exhaust from automobiles and have developed various sensors for the detection of NO_2 [2-6]. Metal oxides are good sensors for the detection of polluting gases [7]. Many researchers

* Corresponding author.
Email address: s.bagul@yahoo.co.in (S.D. Bagul)

Received 9 July 2026
Revised 14 August 2026
Accepted 17 August 2026
Available online 22 August 2026

https://doi.org/10.22034/jams.2026.260304

have attempted to detect NO_2 using various metal oxide-based gas sensors [8].

Nanomaterial-based gas sensors are attracting attention due to their versatile properties, plays key attention of researchers to develop good sensors for the detection of NO_2 gases [9-11]. Metal oxide gas sensors have a large number of advantages over other sensors, such as low cost, easy to operate, small size, and simple integration over the other available sensors [12]. Metal oxides have a large band gap, which can occupy the full spectrum of electronic properties. Metal oxides are thermally and chemically stable materials, which are necessary for repeatability of the sensor response. Metal oxide-based sensors' performance can be enhanced by various parameters such as particle size reduction [13, 14], addition of catalysts [15-17], nanocomposites [18], and porosity of the material [19]. The sensing performance of the metal oxide sensors can be tuned with the operating temperature.

Titanium dioxide (TiO_2) is naturally formed in three different phases: rutile (most stable and substantial form), anatase (tetragonal), and brookite (rhombohedral) [20]. Among these, rutile is the most stable, while anatase and brookite phases are metastable. The anatase phase of TiO_2 shows good gas sensing performance due to its high gas reaction capacity and greater oxygen vacancies [21]. The charge carrier concentrations are higher in the anatase phase compared to the rutile and brookite phases. Titanium dioxide is a versatile material with a wide range of applications: paint [22], sunscreen lotion [23], biomedical [24], humidity sensor [25], gas sensors [26-28], photocatalysts [29], solar cell [30], water treatment [31], electrode for battery [32], etc. Due to its large number of applications, researchers have synthesized TiO_2 in various forms such as thin films, nano powders with different morphologies, nanowires, nanorods, nanotubes, nanoparticles, etc. The properties of the material also depend on the synthesis methods.

TiO_2 is a material that can be easily prepared by using various techniques, such as chemical precipitation [33], sol-gel [34], hydrothermal [35], sonochemical [36], spray pyrolysis [37], electrochemical [38], thermal evaporation [39], etc. Though TiO_2 is synthesized by various techniques, there is still scope to see other methods to prepare and see the effect of the synthesis method on the gas sensing performance of the sensor. In the present study, TiO_2 powder is prepared using ultrasonic atomization and pyrolysis techniques. TiO_2 is a good candidate for a gas sensor due to its thermal and chemical stability.

2. Experimental

2.1. Preparation of Pure TiO_2 hollow microspheres

Titanium trichloride ($TiCl_3$) was used as a precursor for titanium, and in a typical synthesis, a 0.3 M solution of 200 mL of TiCl3 was prepared in double-distilled water. The solution was stirred for 10 minutes at room temperature to get a homogeneous solution and poured into the flask of the ultrasonic atomizer. The ultrasonic atomizer consists of three transducers, each having frequency 2.4 MHz of Mylan France make was used to generate fine mist. The ultrasonic atomizer converts the solution into fine mist and pushes it into a double-zone quartz reactor furnace with an optimized air pressure of 17.5 liters per minute (LPM). The double-zone quartz reactor furnace was used to dry and pyrolyze fine mist particulates. The quartz reactor temperature was optimized and kept at the first zone at 200°C and second zone at 800°C. The glass traps filled with double-distilled water are connected to the rear end of the furnace to collect the powder. The powder preparation system is shown in Figure 1 above. The pushed fine mist was dried in the first zone and pyrolyzed in the second zone of the furnace. The oxidized mist (powder) gets trapped in the glass traps T1, T2, and T3, respectively, away from the furnace. The powder was removed from the traps and collected with the help of a centrifuge machine and dried in a hot air oven at 80°C for 12 hours. The collected powders were respectively named TiO_2_1, TiO_2_T2 and TiO_2_T3. The powder is now ready for further characterization and gas sensor fabrication.

2.2. Fabrication of thick film-based sensor

The sensors were fabricated using the screen-printing method. In a typical process, 100 mg of ethyl cellulose was ground in a mortar pestle and put organic binder to just wet the ethyl cellulose and waited for 20 minutes; after that put 1 gm of oxide powder and mixed it thoroughly to get a fine paste. The paste was screen printed using a screen-printing board and squeezed to fabricate thick films on glass substrates; the thickness was optimized. The films were dried at room temperature for 12 hours and fired at 500°C for 30 minutes to evaporate organic compounds. The electrical

Figure 1. Photograph of ultrasonic atomization and pyrolysis technique.

contacts were made with the help of adhesive silver paste and copper wires.

2.3. Measurements

The XRD machine used for analysis was a RIGAKU MINIFLEX600, having an accelerating voltage of 40 KV and a tube current of 15 mA with a wavelength. λ = 1.5406 Å. The XRD scanning was performed from 20° to 70° at a speed of 2 degrees per minute. The surface topology of the powder was also analyzed by HRTEM with model no. FEI Tecnai G2F3O S-Twin with operating voltage 300 kV. The sample was prepared by dissolving a small amount of powder into ethanol and ultrasonicated for 15 minutes, and then put into a carbon-coated copper grid used as a substrate.

Gas response of the sensors was measured in terms of resistance measured without gas, i.e., in the air atmosphere, and in the presence of exposed gas. The change in resistance gives us the gas response. The gas response was measured with the help of the following equation.

$$Gas\ response\ = \frac{R_a - R_g}{R_g} \quad (1)$$

where, R_a and R_g are the resistance of the sensor in air and in an exposed gas environment, respectively. The resistance of the sensors was measured with the help of an electrometer of KEITHLEY make and model no. 6517A.The gas sensing responses for various gases were measured at an optimum temperature of 250°C for 1000 ppm of gases.

3. Results and discussion

3.1. XRD results

The structural information of the powder was analyzed with the help of XRD. Figure 2 shows the typical XRD patterns of the powder collected in different traps connected to the rear end of the double-zone quartz reactor furnace. The XRD patterns show that the powder consists of mixed phases of anatase TiO_2 with JCPDS card no. 21-1272 and rutile with 21-1276. No other impurity peaks are found in the XRD patterns. As seen from Figure 3, the XRD patterns get broader from T1 to T3; this indicates the particles are sorted by size in different traps. One of the reasons for the XRD pattern broadening may be due to the reduction in the crystallite sizes of the material.

The crystallite sizes, microstrains, and dislocation density of the powders were measured from the XRD patterns and tabulated in Table 1. The results indicate that the crystallite sizes of the material collected in Trap T3 are smaller than the Trap T1 and T2. This may have happened due to the gravimetric trapping effect of the powders in the different traps connected to the rear end of the horizontal quartz reactor furnace. The

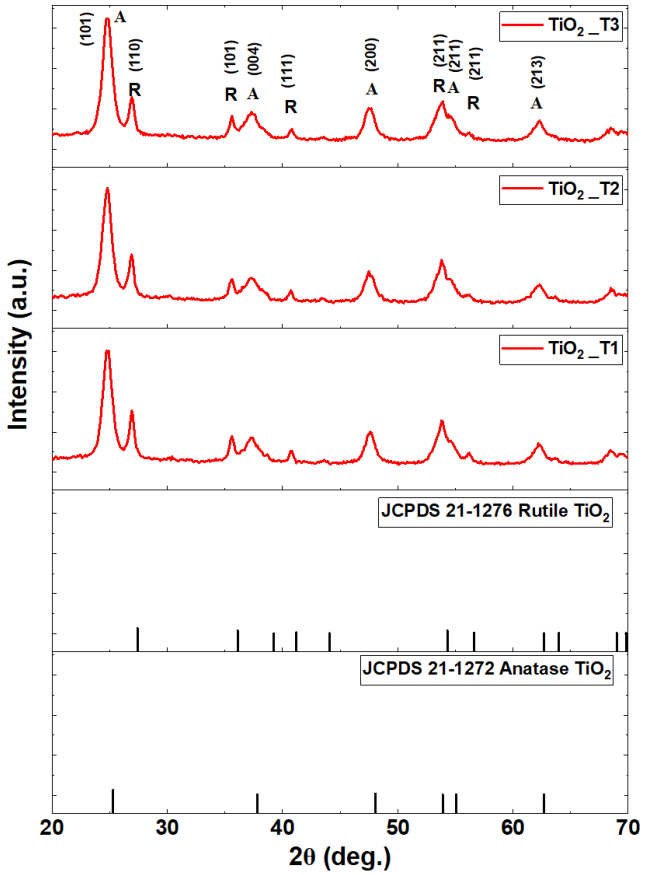

Figure 2. XRD patterns of powder collected at T1, T2 and T3.

microstrains and dislocation density of the material increased from trap T1 to trap T3; this may be due to the reduction in crystallite sizes, which creates more strains

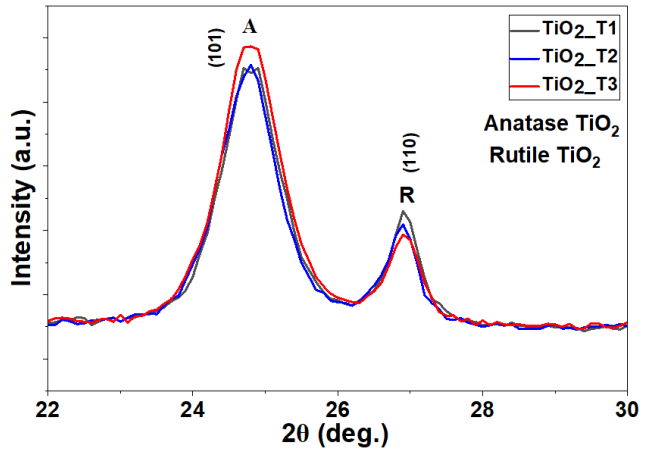

Figure 3. Enlarged XRD patterns from Figure 2.

Table 1. Crystallite sizes, microstrains, and dislocation densities of samples

Sample	Crystallite size (nm) $D = \frac{0.94 * \lambda}{\beta cos\theta}$	Microstrain (Rad) $\varepsilon = \frac{\beta}{4tan\theta}$	Dislocation density (1/nm²) $\delta = \frac{1}{D^2}$
TiO_2_T1	18.692	0.01028	2.862×10^{-3}
TiO_2_T2	15.161	0.02129	4.351×10^{-3}
TiO_2_T3	14.399	0.02243	4.823×10^{-3}

in the crystals. More defects are helpful for gas sensing due to the more active sites created on the surface by the defects of crystallites.

3.2. FESEM Analysis

The surface morphology of the prepared powders was analyzed by a scanning electron microscope. Figure 4 shows the typical FESEM images of the powders. All the particles are seen to be spherical in nature. The microsphere sizes are seen to be reduced from the trap T1, which is closer to the furnace, to the trap T3. These results are analogous to the XRD results. The microspheres may get separated due to the gravitational basis. In this way, the powders of different-sized microspheres of TiO2 were prepared. The average particle size of the powders was measured from the FESEM images and ImageJ software and is shown in Figure 5 below. It indicates that the average particle size of 260.06 nm, 210.67 nm, and 201.05 nm, respectively, for TiO_2_T1, TiO_2_T2, and TiO_2_T3 powders.

3.3. HRTEM Analysis

The typical HRTEM images of the powder collected from trap T3 are shown in Figure 6. The images show that the microspheres consist of smaller particles. The d-spacing was measured using an HRTEM image and ImageJ software and found to be 0.334 nm, corresponding to (101) crystal planes of TiO_2.

3.4. UV-Visible Absorption Analysis

The UV-Visible absorption spectra of the prepared powder were carried out and displayed in Figure 7. The absorption spectra indicate that from Trap T1 to Trap T3, the edge of absorption shifts towards a shorter

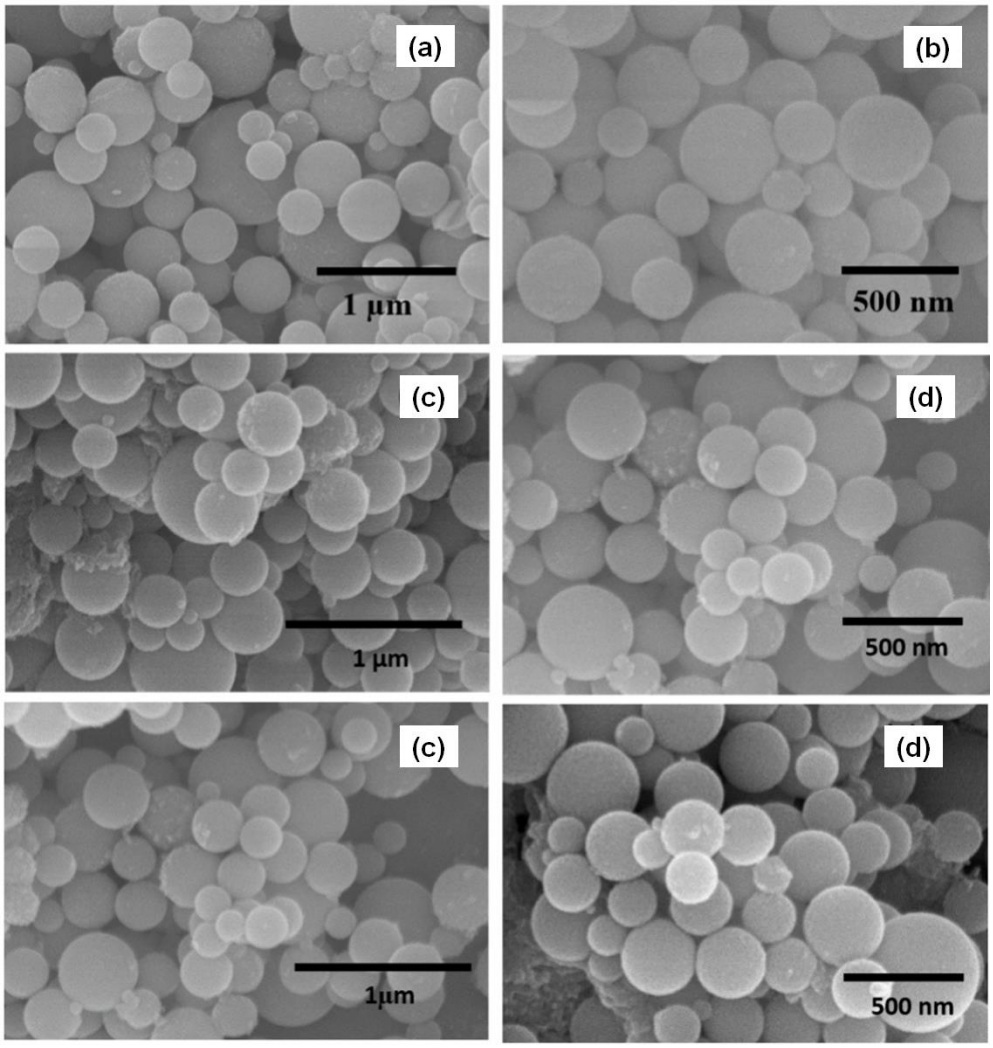

Figure 4. FESEM images of Pure TiO_2_T1 (a and b), TiO_2_T2 (c and d), and TiO_2_T3 (e and f).

wavelength; this shows the blue shift. This may be due to the reduction in particle sizes of TiO_2 particles. The results are analogous to the results shown by XRD and FESEM images. The optical energy band gap is measured from the spectrum, and Tauc plots were found to be 3.21eV, 3.24 eV, and 3.30 eV, respectively, for TiO_2_T1, TiO_2_T2, and TiO_2_T3 powders.

3.5. Photoluminescence (PL) Emission Analysis

The PL emission spectra of the powders were measured and displayed in Figure 8. There seem to be strong emission peaks at 479.29 nm, 515.82 nm, and 582.86 nm. The optical emission is responsible for surface defects [40]. The defects create more active sites, which increases the gas sensing performance of the sensor. The intensity of the peaks increases with the particle size reduction; this may be due to the creation of more active sites on the surface. The higher the surface-to-volume ratio increases the more active sites are created on the surface; also, the creation of vacancies of the metal and oxygen is also responsible for visible emission.

3.6. Thermal analysis

The thermal properties of the powders were analyzed by a simultaneous thermal analyzer (STA). The typical thermogram of the powders is displayed in Figure 9. The thermogram is measured in an oxygen atmosphere, with

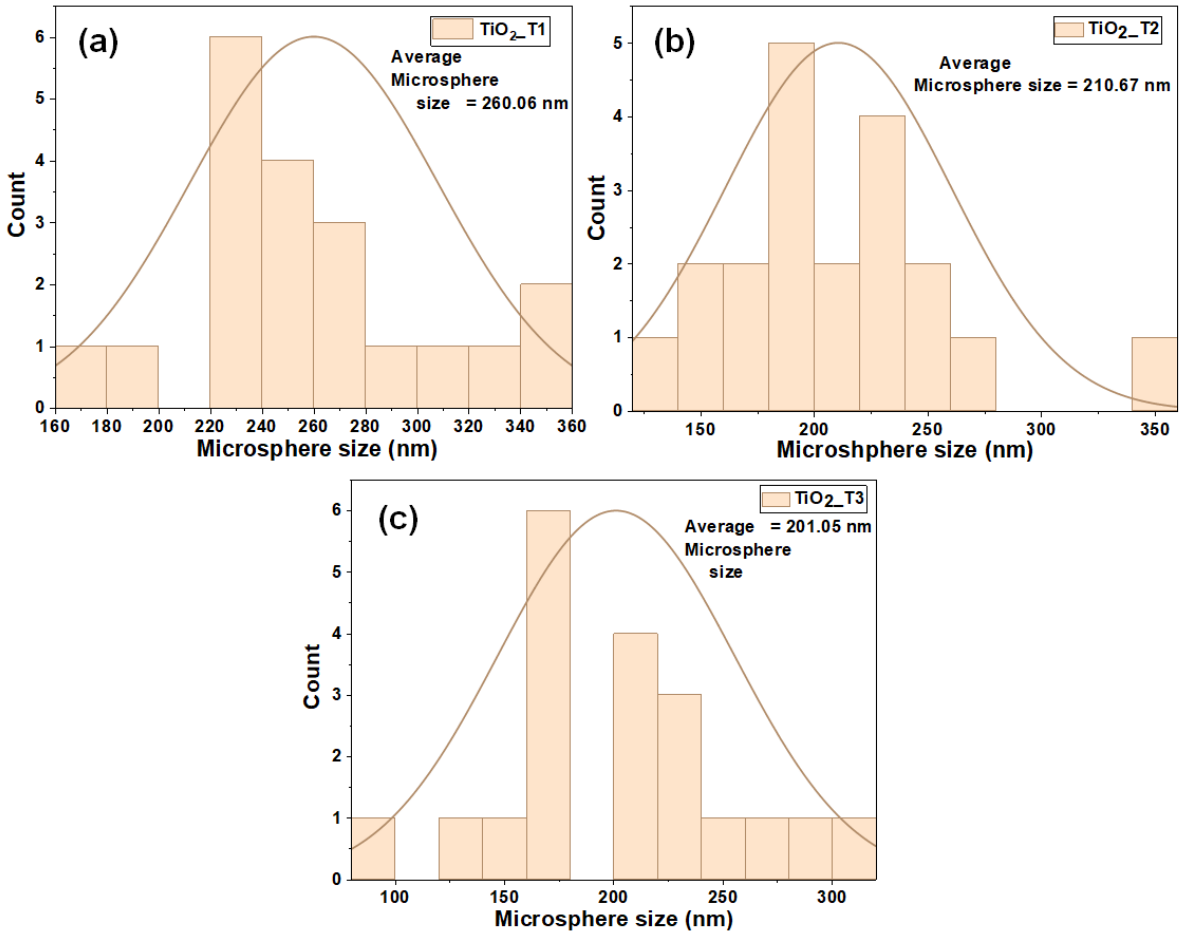

Figure 5. Histogram of the powders collected in different traps.

heating from 50 to 800°C at the rate of 20°C per minute. The thermogram indicates that the materials are thermally stable once heated above 400°C. This indicates that the material is suitable for gas sensor fabrication. The sensor needs material should be thermally more stable [41]. The output properties of the sensor mostly depend on the thermal properties. The powder TiO_2_T3 shows little thermal instability; this may be due to the smaller particle sizes of the powders.

The differential scanning calorimetric (DSC) analysis of the powders was carried out and displayed the DSC curves in Figure 10. The curves indicate that the powders show a strong exothermic peak at 280°C. A stronger

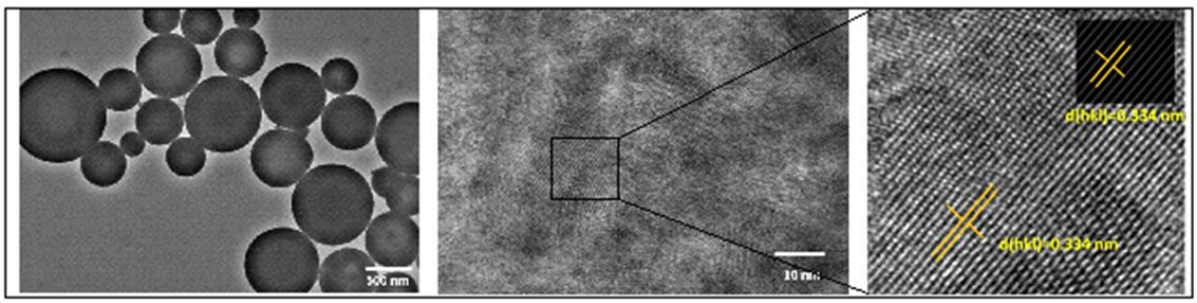

Figure 6. HRTEM images of TiO_2_T3 powder.

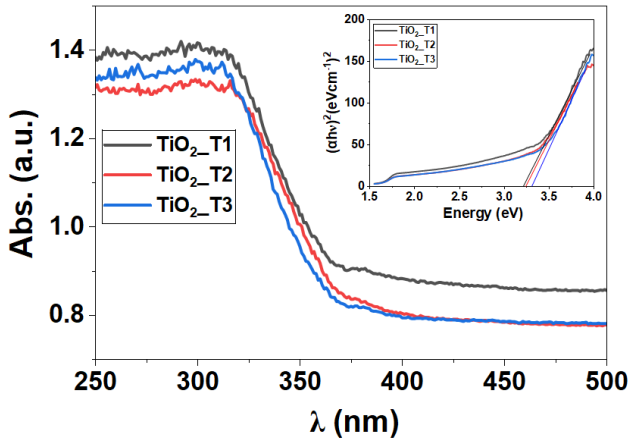

Figure 7. UV-Visible absorption spectra of samples.

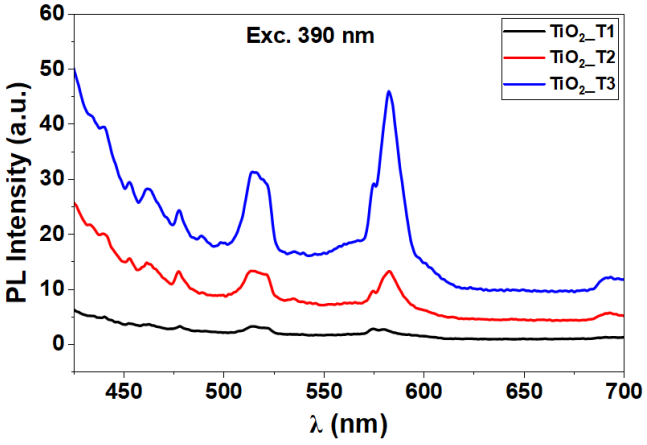

Figure 8. PL emission spectra of the powders.

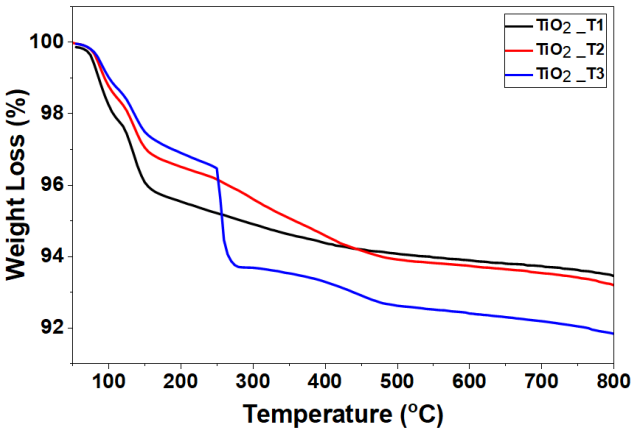

Figure 9. TGA curves of samples.

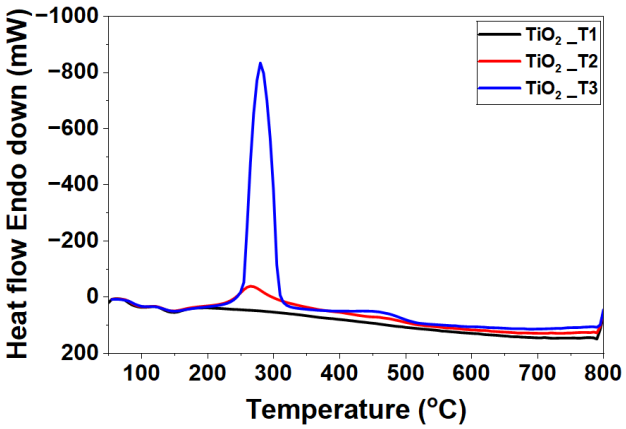

Figure 10. DSC curves of samples.

peak is observed for the powder TiO_2_T3; this may be due to more heat being released for the powder compared to the other powders.

3.7. Gas sensing performance

3.7.1. Current-Voltage (I-V) characteristics of the sensor

The current-voltage characteristics were measured by connecting the sensor across the voltage source and measuring current with respect to the applied voltage at room temperature. The typical I-V graph is shown in Figure 11. The graph shows that the linear nature of I-V indicates the ohmic contact formation.

Figure 12 shows the typical gas response graph for thick film-based TiO_2sensors. The sensors fabricated from the powders show good response to NO_2 gas as compared to other gases. This indicates that the sensors are highly selective and responsive to NO_2 as compared to other gases.

The temperature optimization was carried out by measuring the gas response of the sensors for various operating temperatures. The measured responses are plotted in Figure 13; it indicates that the optimum operating temperature is 250°C. This may be due to more oxygen species being created at the optimum operating temperature as compared to others.

3.7.2. Response recovery of the sensor

The response time of the sensor is defined as the time taken for the sensor to attain 90% of maximum decrease in resistance on injection of target gas. The time taken for the sensor resistance to reach 90% of its initial resistance

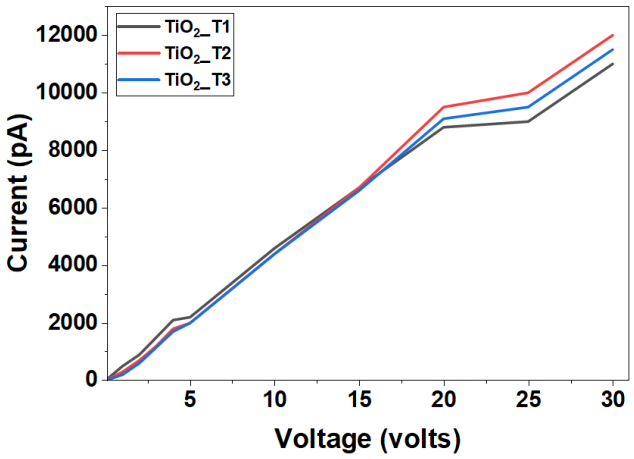

Figure 11. Current-Voltage curves of samples.

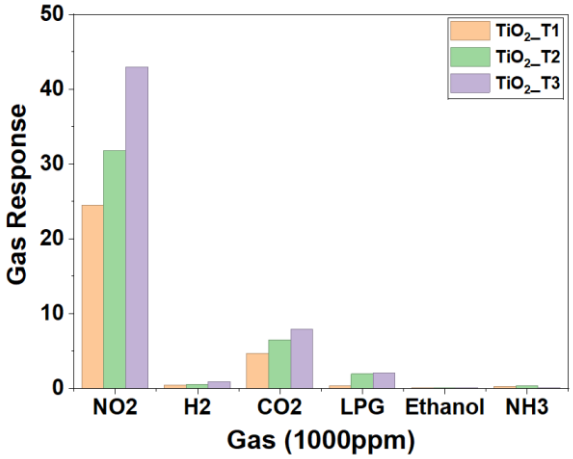

Figure 12. Gas response of sensors.

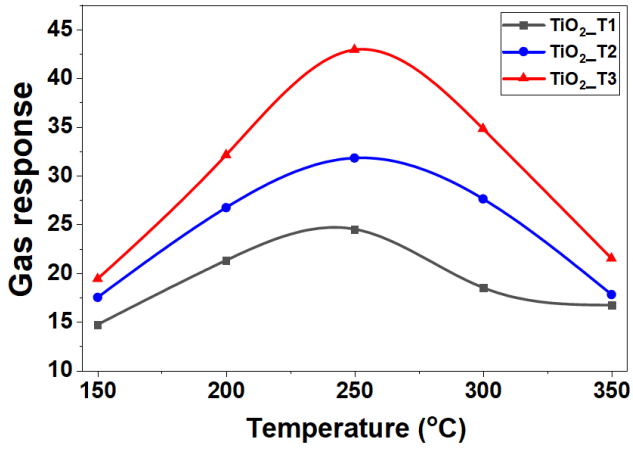

Figure 13. Gas response versus operating temperature of samples.

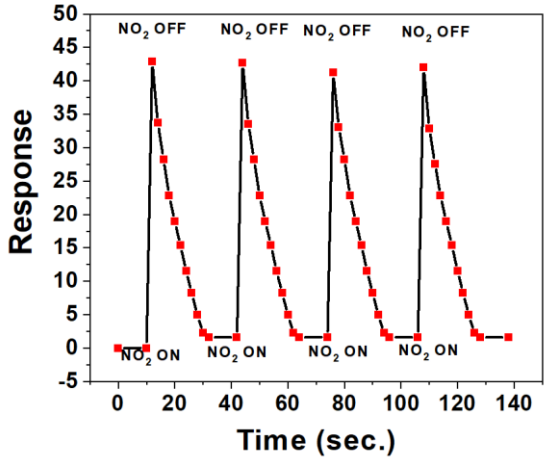

Figure 14. Response-recovery of the TiO_2_T3 sensor.

after the injected gas is switched off is called the recovery time of the sensor. The response recovery of the TiO_2_T3 sensor was measured at the optimum operating temperature of 250°C. Figure 14 shows the typical response recovery of the sensor. The sensor shows quick response and also recovers within 23 seconds; this may be due to the nanocrystalline nature of the particles. The sensor shows good repeatable output response recovery cycles.

4. Conclusions

The TiO_2 microspheres consisting of nanoparticles were successfully prepared by ultrasonic atomization

Table 2. Gas response of TiO_2 thick films

Gas	TiO_2_T1	TiO_2_T2	TiO_2_T3
NO_2	24.5	31.8	42.9
H_2	0.43	0.5	0.9
CO_2	4.7	6.5	7.9
LPG	0.37	1.94	2.04
Ethanol	0.11	0.05	0.07
NH_3	0.23	0.36	0.09

and pyrolysis techniques. The preparative conditions were optimized to get nanocrystalline powder. The powders trapped in different traps were removed and collected. The powders were characterized by various characterization techniques. The XRD patterns of the prepared powder match with the standard anatase with JCPDS card no. 21-1272 and rutile with 21-1276. phases of TiO_2. No other impurity peaks were observed. The powder shows mixed phases of anatase and rutile TiO_2. The XRD patterns clearly indicate that the powder collected at the last trap, i.e., TiO_2_T3, shows broaden XRD pattern as compared to the other powders. This indicates that the powder collected at the last end traps consists of smaller particles. This may be due to the gravimetric effect; the lighter microspheres are pushed towards the next traps. The morphology of prepared powders was analyzed by FESEM; it indicates the powder consists of microspheres. No other morphology was observed in the FESEM images. Powder collected at the last trap shows smaller microspheres. The average microsphere sizes are measured and found to be 260.06 nm, 210.67 nm, and 201.05 nm, respectively, for TiO_2_T1, TiO_2_T2, and TiO_2_T3 powders. The microstructure was also analyzed by HRTEM images and found to be hollow microspheres, as the walls of the microspheres are seen to be dark compared to the center part of the microspheres. The HRTEM images also show that the powder consists of crystalline material. The d-spacing was measured with the help of the HRTEM image and ImageJ software and found to be 0.334 nm, corresponding to the (101) plane of TiO_2.

The optical properties of the powders were analyzed by a UV-Visible absorption spectrophotometer. The energy band gap of the powder was measured from the absorption spectrum and the Tauc plot, found to be 3.21eV, 3.24 eV, and 3.30 eV, respectively, for TiO_2_T1, TiO_2_T2, and TiO_2_T3 powders. There seems to be a blue shift; this may be due to the reduction in particle sizes of the TiO_2 powders. The photoluminescence properties were measured by exciting the powders with 390 nm wavelength, and emission is found in the visible region; this may be due to surface defects, such as oxygen vacancies, point defects, etc. Thermal properties were analyzed by a simultaneous thermal analyzer. The thermograph indicates that the powder is thermally stable. Thermal stability is a requirement for the repeatable operation of the gas sensor. The differential scanning calorimeter (DSC) curves indicate that the powders show one exothermic peak at 280°C. This may be due to more heat being evolved and exhausted at a particular temperature. The gas sensing performance of the sensors was measured and found to be highly sensitive to NO_2 gas as compared to the other gases. The sensor fabricated from TiO_2_T3 powder shows the highest response to NO_2 gas as compared to other sensors. This may be due to the sensor consisting of smaller particles having a high surface-to-volume ratio, which creates more active sites on the surface. The more active sites adsorb more oxygen species, which reduces the resistance of the sensor. When the sensor was exposed to NO_2 gas, which releases more electrons, there was more change in the resistance of the sensor. The gas sensing mechanism is diagrammatically shown in Figure 15. The sensor was fabricated using the screen-printing technique. The powder of TiO_2 consists of microspheres; when it is exposed to the atmosphere at optimum operating temperature, the oxygen species such as O^-, $O^{2-}$and O_2^- is getting adsorbed on the surface by capturing electrons from the sensor; due to this, the resistance of the sensor is increased by a reduction in electrons in the conduction band of the sensor. When it is exposed to NO_2 gas on the sensor at OOT, the NO_2 gas interacts with the oxygen species, giving NO and O2 by

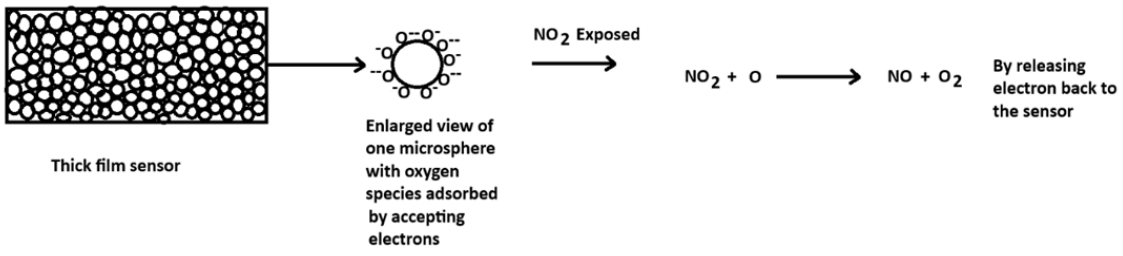

Figure 15. Gas sensing mechanism of the sensor.

releasing electrons back to the sensor. Due to this, the resistance of the sensor decreases by increasing the number of electrons in the conduction band.

The optimum operating temperature was measured and found to be 250°C. This may be because the optimum condition is created at 250°C, where more oxygen species are adsorbed on the surface of the sensor, which produces a large change in resistance of the sensor while exposed to the target gas. The response recovery of the TiO_2_T3 sensor is measured, and the sensor shows a quick response within 2 seconds, reaching its maximum response and recovering within 23 seconds. The sensor also shows good repeatable output characteristics while measuring multiple cycles. The TiO_2 microspherical powder prepared by ultrasonic atomization and pyrolysis technique can be used for the fabrication of an NO_2 gas sensor. The powder preparation technique is simple; it uses ultrasonic atomizers and pyrolyzes the mist to get TiO_2 powders.

Acknowledgments

The author is thankful to Rashtriya Uchchatar Shiksha Abhiyan (RUSA) for providing funding to conduct this research.

Conflict of Interest

The authors declare no conflict of interest.

References

1. S.S. Taha, et al. Comprehensive review of health impacts of the exposure to nitrogen oxides (NOx), carbon dioxide (CO2), and particulate matter (PM). *Journal of Hazardous Materials Advances*, **2025**, *19*, 100771.
2. Y. Mizutani, et al. Improvement of electrochemical NO2 sensor by use of carbon–fluorocarbon gas permeable electrode. *Sensors and Actuators B: Chemical*, **2005**, *108*, 815.
3. A.-M. Andringa, et al. NO2 Detection and Real-Time Sensing with Field-Effect Transistors. *Chemistry of Materials*, **2013**, *26*, 773.
4. A. Paliwal, et al. Room temperature detection of NO2 gas using optical sensor based on surface plasmon resonance technique. *Sensors and Actuators B: Chemical*, **2015**, *216*, 497.
5. K.G. S, et al. Highly sensitive NO2 sensor based on ZnO nanostructured thin film prepared by SILAR technique. *Sensors and Actuators B: Chemical*, **2021**, *335*, 129678.
6. P. Kyokunzire, et al. Systematic Optimization of NO2 Detection Using Activated Carbon-Based Resistive Sensors. *ACS Applied Electronic Materials*, **2025**, *7*, 2349.
7. M. Wang, et al. Highly Sensitive Gas Sensor for Detection of Air Decomposition Pollutant (CO, NO _x): Popular Metal Oxide (ZnO, TiO 2)-Doped MoS 2 Surface. *ACS Applied Materials & Interfaces*, **2024**, *16*, 3674.
8. Q. Li, W. Zeng, and Y. Li. Metal oxide gas sensors for detecting NO2 in industrial exhaust gas: Recent developments. *Sensors and Actuators B: Chemical*, **2022**, *359*, 131579.
9. A. Khort, et al. High-performance selective NO2 gas sensor based on In2O3–graphene–Cu nanocomposites. *Scientific Reports*, **2023**, *13*.
10. S.-Y. Chu, et al. Sensing Mechanism and Characterization of NO2 Gas Sensors Using Gold-Black NP-Decorated Ga2O₃ Nanorod Sensing Membranes. *ACS Sensors*, **2023**, *9*, 118.
11. J.N.O. Amu-Darko, et al. Advanced 2D nanosheet-based gas sensor for sensitive detection of low concentration NO2 gas using In2O3/Ti3C2 layers. *Sensors and Actuators B: Chemical*, **2024**, *407*, 135464.
12. Z. Li, et al. Advances in designs and mechanisms of semiconducting metal oxide nanostructures for high-precision gas sensors operated at room temperature. *Materials Horizons*, **2019**, *6*, 470.
13. T. Kida, et al. Pore and Particle Size Control of Gas Sensing Films Using SnO2 Nanoparticles Synthesized by Seed-Mediated Growth: Design of Highly Sensitive Gas Sensors. *The Journal of Physical Chemistry C*, **2013**, *117*, 17574.
14. L. Liu, et al. Heteronanostructural metal oxide-based gas microsensors. *Microsystems & Nanoengineering*, **2022**, *8*, 85.
15. G. Korotcenkov, et al. The influence of additives on gas sensing and structural properties of In2O3-based ceramics. *Sensors and Actuators B: Chemical*, **2007**, *120*, 657.
16. M.N. Rumyantseva and A.M. Gas'kov. Chemical modification of nanocrystalline metal oxides: effect of the real structure and surface chemistry on the sensor properties. *Russian Chemical Bulletin*, **2008**, *57*, 1106.
17. I.C. Weber and A.T. Güntner. Catalytic filters for metal oxide gas sensors. *Sensors and Actuators B: Chemical*, **2022**, *356*, 131346.
18. G. Korotcenkov and B.K. Cho. Metal oxide composites in conductometric gas sensors: Achievements and challenges. *Sensors and Actuators B: Chemical*, **2017**, *244*, 182.

19. M.A. Han, et al. Effects of porosity and particle size on the gas sensing properties of SnO2 films. *Applied Surface Science*, **2019**, *481*, 133.

20. S.I. Sadia, et al. Crystallographic biography on nanocrystalline phase of polymorphs titanium dioxide (TiO2): A perspective static review. *South African Journal of Chemical Engineering*, **2024**, *50*, 51.

21. S.F. Shaikh, et al. Low-Temperature Ionic Layer Adsorption and Reaction Grown Anatase TiO2 Nanocrystalline Films for Efficient Perovskite Solar Cell and Gas Sensor Applications. *Scientific Reports*, **2018**, *8*, 11016.

22. B.P. Sharma, et al. Optimizing the effect of TiO2 nano powder in water-based paint manufacturing using response surface methodology. *Scientific Reports*, **2025**, *15*, 37072.

23. M. Morsella, et al. Improving the Sunscreen Properties of TiO2 through an Understanding of Its Catalytic Properties. *ACS Omega*, **2016**, *1*, 464.

24. Z. Fei Yin, et al. Recent progress in biomedical applications of titanium dioxide. *Physical Chemistry Chemical Physics*, **2013**, *15*, 4844.

25. Y. Weng, et al. Highly sensitive humidity sensor based on sub-micron level TiO2 flowers structure. *Applied Surface Science*, **2026**, *715*, 164565.

26. N. Chen, et al. TiO2 nanoparticles functionalized by Pd nanoparticles for gas-sensing application with enhanced butane response performances. *Scientific Reports*, **2017**, *7*, 7692.

27. X. Tian, et al. Gas sensors based on TiO2 nanostructured materials for the detection of hazardous gases: A review. *Nano Materials Science*, **2021**, *3*, 390.

28. J. Zhao, et al. The Challenges and Opportunities for TiO2 Nanostructures in Gas Sensing. *ACS Sensors*, **2024**, *9*, 1644.

29. K. Solymos, et al. Photocatalytic and surface properties of titanium dioxide nanoparticles in soil solutions. *Environmental Science: Nano*, **2024**, *11*, 1204.

30. R. Ur Rahman, et al. Synthesis and simulation study of titanium dioxide-based nanomaterial for electron carrier selective contact solar cell. *Inorganic Chemistry Communications*, **2024**, *169*, 112863.

31. C. Han, et al. Titanium dioxide-based antibacterial surfaces for water treatment. *Current Opinion in Chemical Engineering*, **2016**, *11*, 46.

32. H. Shi, et al. Titanium dioxide-based anode materials for lithium-ion batteries: structure and synthesis. *RSC Advances*, **2022**, *12*, 33641.

33. W. Buraso, et al. Synthesis of TiO 2 nanoparticles via a simple precipitation method and photocatalytic performance. *Materials Research Express*, **2018**, *5*, 115003.

34. N. Sondezi, et al. Sol–Gel-Derived TiO2 and TiO2/Cu Nanoparticles: Synthesis, Characterization, and Antibacterial Efficacy. *ACS Omega*, **2024**, *9*, 15959.

35. M. Rehan, X. Lai, and G.M. Kale. Hydrothermal synthesis of titanium dioxide nanoparticles studied employing in situ energy dispersive X-ray diffraction. *CrystEngComm*, **2011**, *13*, 3725.

36. W. Guo, et al. Sonochemical synthesis of nanocrystalline TiO2 by hydrolysis of titanium alkoxides. *Microelectronic Engineering*, **2003**, *66*, 95.

37. M.O. Abou-Helal and W.T. Seeber. Preparation of TiO2 thin films by spray pyrolysis to be used as a photocatalyst. *Applied Surface Science*, **2002**, *195*, 53.

38. G. Sánchez-García, et al. TiO2 nanostructures synthesized by electrochemical anodization in green protic ionic liquids for photoelectrochemical applications. *Ceramics International*, **2023**, *49*, 26900.

39. J.-M. Wu, et al. Thermal evaporation growth and the luminescence property of TiO2 nanowires. *Journal of Crystal Growth*, **2005**, *281*, 384.

40. A. Anjum, et al. Structure and defects-related optical properties of highly (002)-oriented zinc oxide thin films. *Physica B: Condensed Matter*, **2022**, *644*, 414195.

41. H. Chai, et al. Stability of Metal Oxide Semiconductor Gas Sensors: A Review. *IEEE Sensors Journal*, **2022**, *22*, 5470.